

# Nonlinear viscous vortex motion in two-dimensional Josephson junction arrays

T. J. Hagenaars<sup>1</sup>, P. H. E. Tiesinga<sup>1</sup>, J. E. van Himbergen<sup>1</sup> and Jorge V. Jose<sup>1,2</sup>

<sup>1</sup>Instituut voor Theoretische Fysica,

Princetonplein 5, Postbus 80006, 3508 TA Utrecht, The Netherlands

<sup>2</sup>Department of Physics, Northeastern University,

Boston Massachusetts 02115, USA

(December 31, 2021)

## Abstract

When a vortex in a two-dimensional Josephson junction array is driven by a constant external current it may move as a particle in a viscous medium. Here we study the nature of this viscous motion. We model the junctions in a square array as resistively and capacitively shunted Josephson junctions and carry out numerical calculations of the current-voltage characteristics. We find that the current-voltage characteristics in the damped regime are well described by a model with a nonlinear viscous force of the form  $F_D = -(\eta)\underline{v} = \frac{A}{1+B\underline{v}}\underline{v}$ , where  $\underline{v}$  is the vortex velocity,  $(\eta)$  is the velocity dependent viscosity and A and B are constants for a fixed value of the Stewart-McCumber parameter. This result is found to apply also for triangular lattices in the overdamped regime. Further qualitative understanding of the nature of the nonlinear friction on the vortex motion is obtained from a graphic analysis of the microscopic vortex dynamics in the array. The consequences of having this type of nonlinear friction law are discussed and compared to previous theoretical and experimental studies.

PACS numbers: 74.50.+r, 74.60.Ge, 74.60.Jg, 74.70.Mq

## I. INTRODUCTION

Understanding the vortex motion produced by externally applied currents has been an important topic in the study of the transport properties of Type II superconductors in the Abrikosov phase. When vortices are able to move across the system they produce Faraday voltages that are responsible for the I-V characteristics measured experimentally. It has been useful to describe the transport properties of the dilute vortex phase in terms of a phenomenological single vortex equation of motion. An example of this approach is given by the Bardeen-Stephens equation which has been successfully applied to conventional superconductors [1]. A similar approach has been attempted in the description of the transport properties in two-dimensional Josephson junction arrays (JJA) [2-17]. These arrays are 2D lattices of superconducting islands (sites) connected by Josephson junctions (bonds). The unit cells (plaquettes) of these lattices can be, for example, square or triangular. In the JJA case the vortices are represented by eddy current patterns about a plaquette. Although these JJA vortices differ in several important ways from their continuum counterparts, the question that has been addressed by several authors is: To what extent can one use a single macroscopic equation of motion to describe the dynamical properties of vortices in JJA? Further interest in this problem has come from recent experiments in underdamped arrays [11-13]. These arrays were found to show hysteretic features in their I-V characteristics that suggest that vortices behave as particles with a mass [11]. Furthermore, experimental evidence for ballistic vortex motion was reported in triangular arrays [13].

In this paper we concentrate on the friction experienced by a JJA vortex. We investigate this friction in detail by numerical simulation of the dynamics of an array containing one single vortex. The commonly adopted vortex equation of motion assumes a frictional force proportional to the vortex velocity. Our results show that, instead, the friction is a nonlinear function of the vortex velocity that decreases as the velocity increases. We propose a new phenomenological friction law that accounts for the numerical results.

Here we consider the classical regime defined by  $E_J \gg E_c = e^2/2C$ , where  $E_J$  is the Josephson coupling energy and  $E_c$  the charging energy of two islands,  $e$  the electron charge, and  $C$  the capacitance of the junction. In this regime quantum fluctuations are neglected, leaving the phases  $\varphi(r)$  of the Ginzburg-Landau order parameter on the islands as the only dynamical variables. The experiments mentioned above were reported to be in this regime. In this case the JJA are well modelled by the RCSJ model, defined by the total bond current  $i(r;r^0)$ , between nearest neighbor sites  $r$  and  $r^0$

$$i(r;r^0) = i_c [\varphi(r;r^0) - \varphi(r^0;r^0)] + \frac{1}{2} \sin[2\varphi(r;r^0) - A(r;r^0)]; \quad (1)$$

plus Kirchhoff's current conservation conditions at each site. Here the dots represent time derivatives. The three contributions to  $i(r;r^0)$  are the displacement, the dissipative and the superconducting currents, respectively. The phase difference across a junction is  $\varphi(r;r^0)$

$\varphi(r) - \varphi(r^0)$ . The currents are expressed in units of the junction critical current  $I_c$ ; time is measured in units of the characteristic time  $\tau_c = \hbar/(2eR_n I_c)$ , and  $i_c = (I_c/I_p)^2$  is the Stewart-McCumber parameter [18], with the plasma frequency  $\omega_p$  defined as  $\omega_p^2 = 2eI_c/\hbar C$ , and  $R_n$  is the junction's normal state resistance. The bond frustration variable  $A(r;r^0)$  is defined as the line integral of the vector potential  $A$ :

$$A(r; r^0) = \frac{1}{2\pi} \int_{r^0}^r \frac{1}{r'} A(r'; r^0) dr'; \quad (2)$$

with the elementary quantum of flux  $\Phi_0 = hc/2e$ .

It has been suggested that the transport properties emerging from Eq. (1), in the case that the phase configurations in the array contain one vortex, can be described by a classical macroscopic model in terms of a single continuous vortex coordinate  $y$  that satisfies the equation of motion [4,7,9]

$$M \ddot{y} + \gamma \dot{y} = i_b + i_d \sin(2\pi y); \quad (3)$$

where  $M = \frac{2}{\pi} \frac{\Phi_0^2}{J_c}$  and  $\gamma = \frac{2}{\pi} \frac{\Phi_0^2}{J_c}$  for a square array, and  $M = \frac{4}{\pi} \frac{\Phi_0^2}{J_c}$  and  $\gamma = \frac{4}{\pi} \frac{\Phi_0^2}{J_c}$  for a triangular array. This equation assumes that the JJA vortex can be described as a point particle with mass  $M$  that, driven by a (Lorentz) force  $i_b$ , moves through a sinusoidal pinning potential and experiences a viscous damping force with constant viscosity coefficient  $\gamma$ . The vortex mass  $M$  can be calculated [6] by equating the electromagnetic energy stored in the array to a vortex kinetic energy  $\frac{1}{2} M \dot{y}^2$ . The value of the depinning current,  $i_d$ , depends on the underlying lattice geometry. An estimate for  $i_d$  in a square lattice gives  $i_d \approx 0.1$  while for a triangular lattice it is only  $i_d \approx 0.02$  [19].

If one substitutes  $2\pi y$  by  $\phi$  in Eq. (3), one obtains the equation of motion for the phase difference across a single Josephson junction with current bias  $i_b$ , critical current  $i_d$ , shunt resistance  $2R_n$  (square lattice) or  $R_n$  (triangular lattice) and shunt capacitance  $C=2$  (square lattice) or  $C$  (triangular lattice). Eq. (3) has been studied extensively, mostly numerically, and the results show different types of nontrivial behavior depending on the values of the parameters in the equation [18]. The solutions to Eq. (3) exhibit a critical value  $i_b = i_d$  above which the junction is in a nonzero voltage state. In the array case  $i_d$  corresponds to the depinning current above which the vortex moves and a finite voltage is measured. This voltage is proportional to the vortex velocity and arises because the phase differences across the array change in time. When  $M = 0$ , the overdamped case, and for currents  $i_b < i_d$  the vortex is pinned to the lattice and the voltage is zero. For  $i_b > i_d$  the vortex can move under the action of the current and a nonzero voltage state is produced. For  $M \neq 0$  the I-V characteristics resulting from Eq. (3) show hysteretic behavior when the current  $i_b$  is ramped up and down past the depinning current  $i_d$ . If  $M$  is sufficiently large Eq. (3) predicts ballistic vortex motion, in the sense that a high-velocity vortex would continue its motion over many lattice constants when the driving current is switched off. Van der Zant et al. [13] reported experimental evidence of ballistic vortex motion in a region without driving currents in a H-shaped triangular array with  $\kappa_c = 46$ . The quoted  $\kappa_c$  value was computed from the normal state resistance of the junctions. At low temperatures and voltages, the effective  $\kappa_c$ , determined by the quasi-particle resistance, can be orders of magnitude larger [13]. In contrast to this experimental result, in numerical simulations within the RCSJ model, no evidence for ballistic vortex motion has been found [14-17]; a high velocity vortex in an underdamped array does not move more than one plaquette as soon as the driving current is switched off. Furthermore, the calculated I-V characteristics for square arrays show almost no hysteresis near the vortex depinning current for  $\kappa_c = 10$  [16], whereas Eq. (3) would yield a substantial hysteretic behavior.

In trying to understand this discrepancy between experimental and theoretical studies an additional dissipative mechanism, arising from the coupling of the vortex to spin waves

or plasma oscillations, has been shown to give rise to a nonzero vortex viscosity in the completely underdamped limit ( $\gamma_c = 1$ ) [15]. This would invalidate the model (3) in this limit, leading to very small mean free paths over which vortices come to rest if the driving current is switched off, even in highly underdamped arrays. The enhanced viscosity has also been measured experimentally in Ref. [11]. Nevertheless it was suggested there that the vortices might still move ballistically in a current-free region at low velocities.

In this paper we carry out a systematic comparison between the results for the I-V characteristics obtained from simulations of JJA described by Eq. (1) and the I-V characteristics obtained from an equation of the form given in Eq. (3). The analysis is carried out for a range of  $\gamma_c$  values. We find that an equation of the form of Eq. (3) is not representative of the JJA results. Instead we find strong quantitative evidence that an equation that yields a rather good fit to the JJA results is

$$M(\gamma_c)y + \frac{A(\gamma_c)}{1 + B(\gamma_c)y} y = i_b + i_d \sin(2y): \quad (4)$$

Here the constants  $A$ ,  $B$  and  $M$  are found to be weakly dependent functions of  $\gamma_c$ . This is the main result of this paper. We note that the linear friction law given in Eq. (3) has to be modified in a nonlinear way to account for the JJA results. This nonlinear dependence on the vortex velocity applies in particular to the range  $\gamma_c = 0$  up to  $\gamma_c = 100$ . This change to a nonlinear dissipation law raises some important questions, for example, how to introduce temperature effects at the phenomenological level [20]. We will discuss other important consequences emerging from this nonlinear viscosity law later in the paper.

The outline of the paper is as follows. In Section II we discuss the calculational algorithm used to compute the I-V characteristics from Eq. (1). In Section III we present the bulk of our results for the I-V characteristics together with the fitting analyses that lead to the result given in Eq. (4). In this section we also discuss the microscopic aspects of the vortex motion in the array by analyzing the current distributions of the vortex as a function of time. Section IV contains our conclusions together with a comparison to previous experimental and theoretical work.

## II. CALCULATIONAL APPROACH

In this paper we are interested in calculating the dynamical response of an array of Josephson junctions driven by a constant d.c. current. The set of nonlinear dynamical equations of motion given in Eq. (1) can be efficiently integrated using a fast Fourier transform algorithm [21].

In our simulations we use a square lattice (with a lattice constant set equal to unity) with periodic boundary conditions (pbc) along the y-direction while the current is fed in and taken out along the x-direction (see Fig. 1). Hence a vortex tends to move in the y-direction. The total number of plaquettes along the x- and y-directions are denoted by  $N_x$  and  $N_y$ , respectively, whereas the total number of sites is  $L_x = L_y$ , with  $L_x = N_x + 1$  and  $L_y = N_y$ . Most of the results presented in this paper correspond to systems with  $L_x = L_y$ . However, these results do not change significantly when considering systems with  $L_x \neq L_y$ . In fact, if  $L_x$  is not smaller than 8, the weak finite size effects encountered in our calculations are mainly governed by the vortex motion along the y-direction.

The vorticity  $n(R)$  of a plaquette  $R$  can be defined as (see for instance the Appendix of Ref. [15])

$$2n(R) = 2f + \sum_{P(R)} (\theta(r;r^0) - 2A(r;r^0)) \quad (5)$$

Here  $P(R)$  denotes an anticlockwise sum around the plaquette  $R$  and the gauge invariant phase difference  $\theta(r;r^0) - 2A(r;r^0)$  is taken between  $-$  and  $+$ . The frustration parameter  $f$  measures the average flux piercing a plaquette, measured in units of  $\phi_0$ . Physically, vortices in JJA can be seen as eddy currents in the current flow pattern. If there is only one vortex in the array, then there is one plaquette, say  $R_0$ , with vorticity  $n(R_0) = 1$  while all other plaquettes have zero vorticity. We will call  $R_0$  the core of the vortex. In a JJA with pbc the phase configurations corresponding to a single vortex in the middle column of the array cannot be written down as easily as in an array with free boundaries. We construct a single vortex configuration with a method used previously in Ref. [8]. It allows for a direct calculation of the phase configuration in terms of the vorticities  $n(R) \in \mathbb{Z}$  once a gauge choice for the  $A(r;r^0)$  and a choice for one of the phases  $\theta(r)$  has been made. Here we are mainly interested in understanding the one-vortex dynamics and thus we concentrate on this case throughout the paper.

We take the frustration equal to  $f = 1/N_x N_y$  so that the single vortex we introduce in the middle column of the array has a current pattern symmetric around that column. The single vortex equation of motion proposed in Eq. (3) or Eq. (4) describes a continuous motion in the  $y$ -direction, whereas the location of a vortex as determined from the phase configurations is discrete and undetermined within the vortex core. Therefore, when making comparisons between the vortex velocity, defined in terms of the microscopic phases, to that obtained from the coarse grained vortex variable  $y$ , we need to compare time averaged quantities. The vortex velocity is directly related to the time average of the voltage  $V(t)$  across the array in the  $x$ -direction, where  $V(t)$  is defined as

$$V(t) = \frac{L_x}{L_y} \frac{d}{dt} [\theta(L_x - 1; y) - \theta(0; y)] \quad (6)$$

according to the Josephson relation. Time is again measured in units of  $1/\phi_0$ , and  $V(t)$  is measured in units of  $R_n I_c$ . Each time the vortex has travelled over a distance  $N_y$  the total phase difference across the array has changed by  $2\pi$  and therefore the vortex velocity  $v$  is given by

$$v = \frac{1}{2} V \quad (7)$$

where  $V = \langle V(t) \rangle$ .

Another quantity of interest in describing the vortex dynamics is the current vorticity around a plaquette defined as

$$C(R;t) = \sum_{P(R)} i(r;r^0;t) \quad (8)$$

An important difference between the vorticity  $n(R;t)$  and  $C(R;t)$  is that the former is an integer, while the latter is a continuous function describing the vortex as an eddy current

pattern extending outside the vortex core. One interesting quantity to look at is the "center of mass" of the current vorticities

$$\Upsilon_v = \frac{\sum_{R_y} R_y C(R_y)}{N} = \frac{\sum_{R_y} R_y D(R_y)}{N} \quad (9)$$

with

$$D(R_y) = \sum_{R_x} C(R_x) \quad (10)$$

The normalization factor  $N$  has an unusual form depending on the pbc assumed in our calculations. It is determined by the requirement that  $\Upsilon_v$  has to change one unit if the current vorticity configuration is shifted one plaquette. For two current vorticity configurations  $C(R)$  and  $C^0(R)$  shifted by exactly one plaquette with respect to each other, we get

$$\begin{aligned} N &= \sum_{R_y} \sum_{R_x} R_y D^0(R_y) - \sum_{R_y} \sum_{R_x} R_y D(R_y) \\ &= \sum_{R_y} D(R_y) - L_y D(L_y - 1) \end{aligned} \quad (11)$$

By taking large enough lattice sizes, one can ensure that the quantity  $N$  is essentially constant for a range of positions of the vortex core in the middle of the coordinate system. In this region  $\Upsilon_v$  shows steps with integer height magnitudes.

### III. RESULTS

In this section we present the evidence we have found that allows us to conclude that a vortex in a JJA moves with a nonlinear viscosity law, at least in the overdamped ( $\gamma_c = 0$ ) to damped ( $\gamma_c = 100$ ) regime. We start by considering the overdamped case, in which there are no shunt capacitors, and therefore there is no spin-wave dissipation channel. Next we will discuss the results for values of  $\gamma_c$  up to 100.

#### A. Nonlinear viscosity in the $\gamma_c = 0$ case

Fig. 2 shows a typical I-V characteristic computed for a  $32 \times 32$  array with one vortex ( $f = 1/N_x N_y = 1/992$ ) and with  $\gamma_c = 0$ . In order to compare with the result from Eq. (3), we have plotted the vortex velocity as defined in Eq. (7) versus the current. The results for the I-V characteristics for larger lattices are practically the same, as we will discuss in more detail below. For currents  $i_b \leq 0.10$ , the vortex is pinned by the lattice and thus the measured voltage is zero. Above  $i_b = 0.10$ , the vortex is depinned from the lattice by the current and its motion gives rise to a nonzero voltage. Up to approximately  $i_b = 0.97$ , the time-averaged vortex velocity gradually increases and so does the measured voltage across the array. This is the regime where the phenomenological equation of motion must apply and thus we call the range  $i_b \in [0; 0.97)$  the vortex regime. At  $i_b = 0.97$  we enter a current regime in which eventually all individual junctions in the current direction perform phase slips.

In Fig. 2 we also show, as a continuous line, the result for the I-V characteristic assuming the validity of Eq. (3), with the identification of the parameters as deduced in Refs. [5,6,9]. In the  $M = 0$  case considered here the known analytic expression for the I-V characteristic is given by,

$$v = \frac{1}{R_{1/2} \frac{1}{y} dy} = \frac{q \sqrt{i_b^2 - i_d^2}}{i_b^2 - i_d^2} : \quad (12)$$

In Fig. 2 we observe that the vortex equation of motion seriously underestimates the time-averaged voltage almost everywhere in the vortex regime. There is quantitative agreement with the calculated results only for bias currents very close to the depinning current. More interestingly, we observe a qualitative difference between the two curves. Whereas the viscosity in Eq. (3) is constant the simulations show an effective viscosity which decreases with increasing vortex velocity. This leads us to propose as a model a vortex equation of motion of the form ( $\zeta_c = 0$ ),

$$\langle y \rangle \dot{y} = i_b + i_d \sin(2 \langle y \rangle); \quad (13)$$

with a velocity-dependent viscosity  $\zeta = \langle y \rangle$ . We have found that the functional form for  $\langle y \rangle$  that fits our results in the vortex regime quite well reads,

$$\langle y \rangle = A(1 + B \dot{y}) : \quad (14)$$

where the sign of  $\dot{y}$  is taken positive and  $A$  and  $B$  are parameters determined by fitting the array results to this form. As in the constant viscosity case we can analytically evaluate the result for the I-V characteristics yielding,

$$v = \frac{q \sqrt{i_b^2 - i_d^2}}{A + B \frac{q \sqrt{i_b^2 - i_d^2}}{i_b^2 - i_d^2}} : \quad (15)$$

The top curve in Fig. 3 shows a fit using Eq. (15) in the current range  $i_b = 0.10$  to  $i_b = 0.80$ , to the  $\zeta_c = 0$  I-V characteristic obtained from the simulations of a  $32 \times 32$  array. The values for the parameters are  $A = 2.67$  and  $B = 1.80$ . To indicate the error bars of these values, we mention that, if we fit the form (15) to the simulation results in the range  $i_b = 0.10$  to  $i_b = 0.70$ , the fitted values for  $A$  and  $B$  are approximately 0.5% and 2.0% larger, respectively.

To check on a possible size dependence of these results we carried out the same analysis for lattices of sizes  $64 \times 64$  and  $128 \times 128$ . We find that the I-V characteristics leads to essentially the same results for currents in the range  $i_b \in (0.10; 0.80)$ . Representative results from the fits for  $16 \times 16$  and  $32 \times 32$  arrays are given in the inset of Fig. 3. The results for the two larger sizes are essentially indistinguishable, within their error bars, from the ones shown for  $32 \times 32$  arrays.

We conclude at this stage that the  $\zeta_c = 0$  results are rather well described by the phenomenological Eqs. (13) and (14). In the inset of Fig. 5 we show the comparison between the friction force  $F_D$  in the constant viscosity model (Eq. (3)) and the one proposed here (Eq. (4)) using the  $\zeta_c = 0$  values for the parameters  $A$  and  $B$  derived from our fits.

## B. Nonlinear viscosity in the $\kappa \neq 0$ case

We move now to discuss the changes that occur when  $\kappa \neq 0$ . We solve the phenomenological vortex equation of motion, Eq. (4), numerically to compare to the results obtained from solving the JJA equations. In Fig. 3 we show the results for the I-V characteristics of a  $32 \times 32$  array in the vortex regime for  $\kappa = 0; 1.2; 2; 3$  and 25. We also show the fits to the array results using the form given in Eq. (15). Nonlinear behaviour persists for values of  $\kappa$  up to 50. The fits for small  $\kappa$  are of the same quality as for  $\kappa = 0$ . Note that we take  $M(\kappa) = 0$  in these fits, although Eq. (3) suggests a non-zero mass  $M$  as soon as  $\kappa \neq 0$ . Including a mass  $M$  as a parameter, as in equation (4), does not result in a better fit of the nonlinearity in the vortex regime. The choice  $M(\kappa) = 0$  is corroborated by the fact that we do not find any measurable hysteresis near the depinning current in the simulated I-V characteristics for Stewart-McCumber parameters even up to  $\kappa = 35$ , in agreement with the results for  $\kappa = 10$  reported previously in Ref. [16]. The puzzling conclusion is then that, even when the microscopic equations of motion have a "mass" term, the phenomenological vortex equation of motion behaves as if the vortex mass is zero or very small. In the inset of Fig. 3 we show the  $\kappa$  dependence of the parameters  $A$  and  $B$  for  $\kappa$  up to 4. We note that  $A$  increases slightly with  $\kappa$  while  $B$  decreases slightly. This trend indicates that the viscosity becomes "more" linear as  $\kappa$  increases. This trend can be understood as being a consequence of the "spin-wave friction" mechanism that sets in at  $\kappa > 0$  and leads to an enhancement of the linear viscosity. An approximate estimate of the linear viscosity in this regime presented in Ref. [15] led to a rise roughly proportional to  $\frac{1}{\kappa}$ . The same trend was found experimentally and a semi-quantitative explanation of the results was given in the second reference of [11].

For lattices of size  $8 \times 8$  and larger one needs  $\kappa$  values of the order of 100 to detect small hysteresis loops near the depinning current. For these lattice sizes, no hysteresis is measured up to  $\kappa = 35$  in our , using a current grid as small as  $3 \times 10^{-6}$ . We have found, however, that for a small array of size  $4 \times 4$ , a very small hysteresis loop is visible in this  $\kappa$  regime which resembles in shape the ones obtained using Eq. (3). In Fig. 4 we show these hysteresis loops for  $\kappa$  values between 7 and 13. Note that all the I-V characteristics have the same depinning current while ramping the current up whereas they have different zero voltage intercepts when lowering the currents.

In Fig. 5 we show the vortex regimes of the I-V characteristics for  $\kappa$  values up to 100 on a  $32 \times 32$  lattice. Here we only show the result from ramping up the current, thereby omitting the small hysteresis loops below the depinning currents for  $\kappa = 50$  and 100. For  $\kappa = 7$ , we find sharp jumps in the voltage. The vortex regime ends at these jumps, which are believed to be due to switching of rows of junctions to the resistive state. This row-switching behavior has been seen before in experiments [11,12,22] and in simulations [14,17,23]. In this figure we note a crossover from a nonlinear to a linear viscosity regime as  $\kappa$  increases. At  $\kappa = 100$  the vortex regime of the I-V characteristic is nearly linear for  $i_b > 0.25$  and can be extrapolated through the origin (the step-like structure of the I-V characteristics in the upper half of the vortex regime corresponds to interference of the vortex with its periodic image, as was explained in Ref. [15], and will disappear if we consider a system with larger  $L_y$ ). For  $\kappa = 50$  a similar extrapolation does not intersect the origin, so the friction is still nonlinear. We note that the range of applicability of the nonlinear viscosity model given in



Eq. (4) covers some of the  $\zeta_c$  values reported in the experiments in Refs. [11].

### C. Nonlinear viscosity in triangular arrays

All of the calculations described above were performed in square lattices. Recently Yu and Stroud carried out calculations of the I-V characteristics in triangular arrays [17]. We have reanalyzed their results in light of our nonlinear viscosity model given in Eq. (4). In Fig. 6 we show the corresponding  $\zeta$  to their  $\zeta_c = 0$  results for the I-V characteristic of an  $8 \times 8$  lattice with the current biased in the  $[101]$  direction. The  $\zeta$  to the parameters  $A$  and  $B$  yield the results 7.67 and 2.47, respectively. From these numbers we conclude that the magnitude of the viscosity is roughly 2.8 times as large as in the square lattice case, while the nonlinearity parameter  $B/A$  is smaller. We note that a theoretical prediction of a factor of two for  $A$  between the square and triangular lattices was made in Ref. (9).

### D. Microscopic vortex motion

It is interesting to directly study the time evolution of the vortex motion across the array in order to further understand the nature of the nonlinear viscosity suggested by the phenomenological microscopic model given in Eq. (4). We concentrate here on the  $\zeta_c = 0$  case.

In Fig. 7(a) we show current vorticity distributions of a vortex for  $i_b = 0.11$ , slightly above the depinning current, at different times. We observe that the vortex motion has essentially two time scales, a slow and a fast one. In the slow regime the vortex does not move much while it gets deformed by the applied current. Subsequently the vortex moves fast until it gets stuck again and the stretching process repeats itself. This type of stick-slip-like motion is reflected in the nonlinearity of the viscosity. The decrease of the viscosity with increasing velocity is analogous to the behaviour of the kinetic friction coefficient between dry surfaces in the stick-slip phase, which is likely to be generic for frictional dynamics at low speeds [24]. As shown in Fig. 7(b) the qualitative motion of the vortex remains the same for  $i_b = 0.6$ , although the quantitative values for the slow and fast times have become smaller.

In Fig. 8 we show results for the time-dependent voltage  $V(t)$  (full line) and the normalized center of mass vortex velocity (dashed line) defined as

$$\mathbf{v}(t) = \frac{d}{dt} \mathbf{Y}_v; \quad (16)$$

where  $\mathbf{Y}_v$  is given in Eq. (9), for three values of  $i_b$ . In order to ensure a constant value for the normalization factor  $N$  in a wide range of vortex positions we choose a lattice of size  $8 \times 64$ . We observe that in both the  $V(t)$ - and the  $\mathbf{v}(t)$ -curves, the amplitude of the oscillations around the average value decreases with increasing the bias currents. If we interpret the quantity  $\mathbf{v}(t)$  as a coarse-grained vortex velocity, the physical meaning of this result is that the pinning force decreases when the vortex velocity increases. To check this interpretation we extract the pinning barrier from the simulations, by measuring the variation in the array energy given by

$$E = \sum_{\langle r; r^0 \rangle} \cos[ (r; r^0) - 2 A (r; r^0) ]: \quad (17)$$

We find that the pinning barrier shows a similar decrease as a function of the (time-averaged) vortex velocity. Under the assumption that the pinning force in the array is proportional to the pinning energy barrier, we conclude that indeed the amplitude of the pinning force decreases when the vortex velocity increases, in accordance with the interpretation of the quantity  $\Psi$ . We can qualitatively relate this result to the current vorticity snapshots shown in Fig. 7: for larger currents the vortex moves faster, the current vorticity spreads out over more plaquettes and the pinning at the core plaquette becomes less effective.

#### IV. CONCLUSIONS AND COMPARISON TO PREVIOUS WORK

In this paper we have proposed a phenomenological vortex equation of motion that fits well the I-V characteristics obtained from solving the full set of JJA microscopic dynamical equations. The main difference with previous studies is that our proposed equation of motion has a nonlinear velocity dependent viscosity that decreases as the velocity increases. The validity of this description covers the range from overdamped to damped regimes as defined by the Stewart-McCumber parameter, and it applies to square as well as to triangular lattices. We also have found that for  $\beta_c \approx 35$  the I-V characteristics indicate that the vortex moves as if its inertial mass is zero, or at most very small (no hysteresis at depinning). As  $\beta_c$  increases the nonlinearity of the viscosity slowly decreases at the same time that the linear term slowly increases. We will now discuss the above results in the light of previous experimental and theoretical studies.

Experimentally, evidence for the nonlinear viscosity can be seen in the I-V characteristics reported in Refs. [11,12]. However, the I-V characteristics results measured in Ref. [11] for an almost overdamped triangular array do not show evidence for a nonlinear viscosity, whereas in our simulations it is in the overdamped case that the nonlinearity is dominant (see Fig. 5).

On the theoretical side, Eckern and Sonin [9] derived a general vortex equation of motion in the continuum limit. In the adiabatic, or small vortex velocity limit, this equation reduces to the model of Eq. (3) without the sinusoidal pinning force. This equation of motion is believed to take into account the spin-wave friction occurring when  $\beta_c \neq 0$ , as found in Ref. [15]. Here we will focus on the  $\beta_c = 0$  case, in which the equation of motion also provides corrections to Eq. (3) beyond the adiabatic limit. Taking a constant vortex velocity  $v$ , for a constant current bias, for  $\beta_c = 0$  the vortex equation of motion reduces to

$$v \int d^2 k \frac{k_x^2 e^{-k^2/2}}{k^2 (1 + v^2 k_y^2)} = 2 i_b: \quad (18)$$

Here the integral in  $k$ -space is over the two-dimensional plane. The vortex velocity  $v$  is taken along the  $y$ -direction. The exponential in the integrand provides a smooth cutoff for large  $k$ . An alternative cutoff used in Ref. [15] consists of replacing the exponential in the integrand by the two-dimensional Heaviside function

$$(\delta(k_x - j) - \delta(k_y - j)): \quad (19)$$

Note that in Eq. (18) we cannot add a sinusoidal pinning force, as this would be inconsistent with the constant-velocity assumption. However, the inclusion of the pinning potential, being most important in producing a finite depinning current, would barely affect the higher-velocity part of the I-V characteristics, where the nonlinearity in Eq. (18) is most pronounced.

In Fig. 9 we show the I-V characteristics computed from Eq. (18), with the exponential  $k$ -cutoff, and for the cutoff given in (19). Both curves intersect the origin, because the lattice pinning potential is absent in (18). We note that the inclusion of non-adiabatic effects in this equation of motion gives rise to a viscosity that decreases with increasing velocity. Although there is an improvement in the higher-velocity part of the I-V characteristic when compared to the linear viscosity vortex equation of motion, Eq. (3), the predictions of the continuum model still deviate qualitatively from the full (lattice) calculations. We note that the higher-velocity component of the I-V characteristic depends crucially on the choice of high-momentum cutoff in Eq. (18).

This work has been motivated in part by the issue of ballistic vortex motion. The phenomenological vortex equation of motion presented in this paper attributes a mass  $M(\phi) = 0$  to the vortex in square arrays in the regime of  $\phi < 35$ . This is a consequence of the absence of hysteresis in the I-V characteristic in this regime, also reported in Ref. [16]. This means that the electromagnetic energy stored in the shunt capacitors does not represent a kinetic energy for the vortex in this regime, at least not in the way suggested by the model Eq. (3). This detracts from the idea behind the possibility of ballistic vortex motion in JJA described by the RCSJ model.

In a separate argument, the enhancement of the viscosity with increasing  $\phi$ , leads to very small path lengths over which a vortex with high initial velocity loses its assumed kinetic energy. The enhancement of the viscosity was also measured experimentally [11]. It has been explained in Refs. [11,15] in terms of an additional friction mechanism due to coupling of the vortex to plasma oscillations. It was also suggested in Ref. [9] that this coupling would not prevent ballistic vortex motion in a small velocity window in triangular arrays. Recent simulations [17] of triangular arrays did not show such a velocity window in the parameter range considered ( $0 < \phi < 1000$ ). However, one may need much larger values of  $\phi$  to possibly see ballistic vortex motion [13].

For the discrepancy between the results of the experiment of Van der Zant et al. [13] and that of the simulations based on the RCSJ model, one possible explanation suggested recently in Ref. [10] involves the discreteness of the charges in the array. The clarification of this problem needs further experimental and theoretical study. With regard to the nonlinear vortex viscosity found in our work, establishing a direct connection between the microscopic and the phenomenological description represents a difficult problem for future study.

#### ACKNOWLEDGMENTS

We thank U. Geigenmüller for useful suggestions about the paper and we thank him and H. van der Zant and J. B. Sokoloff for illuminating conversations. This work was part of the research program of the "Stichting voor Fundamenteel Onderzoek der Materie (FOM)", which is financially supported by the "Nederlandse organisatie voor Wetenschappelijk Onderzoek (NWO)". The work of J.V.J. was partially supported by NSF grant DMR-9211339.

## REFERENCES

- [1] M. Tinkham, Introduction to superconductivity, McGraw-Hill, New York 1975.
- [2] For recent reviews see, Proceedings of the 2nd CTP Workshop on Statistical Physics: KT Transition and Superconducting Arrays, Edited by D. Kim, et al. (Min Eum Sa, Seoul, Korea, 1993).
- [3] A.J. Larkin, Yu.N. Ovchinnikov, and A. Schmid, Physica 152B, 266 (1988).
- [4] U. Eckern and A. Schmid, Phys. Rev. B 39, 6441 (1989).
- [5] U. Eckern, in Applications of Statistical and Field Theory Methods to Condensed Matter, Vol 218 of NATO Advanced Studies Institute, Series B: Physics, edited by D. Baeriswyl et al. (Plenum, New York, 1990), p. 311.
- [6] M.S. Rzchowski, S.P. Benz, M. Tinkham, and C.J. Lobb, Phys. Rev. B 42, 2041 (1990).
- [7] T.P. Orlando, J.E. Mooij, and H.S.J. van der Zant, Phys. Rev. B 43, 10218 (1991).
- [8] H. Eikmans and J.E. van Himbergen, Phys. Rev. B 45, 10597 (1992).
- [9] U. Eckern and E.B. Sonin, Phys. Rev. B 47, 505 (1993).
- [10] R. Fazio, A. van Otterlo, and G. Schon, to be published in Europhys. Lett. (1994).
- [11] H.S.J. van der Zant, F.C. Fritschy, T.P. Orlando, and J.E. Mooij, Phys. Rev. Lett. 66, 2531 (1991); and Phys. Rev. B 47, 295 (1993).
- [12] T.S. Tighe, A.T. Johnson, and M. Tinkham, Phys. Rev. B 44, 10286 (1991).
- [13] H.S.J. van der Zant, F.C. Fritschy, T.P. Orlando, and J.E. Mooij, Europhys. Lett. 18, 343 (1992).
- [14] P.A. Bobbert, Phys. Rev. B 45, 7540 (1992).
- [15] U. Geigenmüller, C.J. Lobb, and C.B. Whan, Phys. Rev. B 47, 348 (1993).
- [16] W. Yu, K.H. Lee, and D. Stroud, Phys. Rev. B 47, 5906 (1993).
- [17] W. Yu and D. Stroud, preprint, to appear in Phys. Rev. B (1994).
- [18] D.E. McCumber, J. Appl. Phys. 39, 3113 (1968); W.C. Stewart, Appl. Phys. Lett. 12, 277 (1968).
- [19] C.J. Lobb, D.W. Abraham, and M. Tinkham, Phys. Rev. B 27, 150 (1983).
- [20] See for example: N.G. van Kampen, Stochastic Processes in Physics and Chemistry, North-Holland, Amsterdam 1983.
- [21] H. Eikmans and J.E. van Himbergen, Phys. Rev. B 41, 8927 (1990); A similar but even faster algorithm was used in D. Domínguez, J.V. José, A. Karma, and C. Wiegko, Phys. Rev. Lett. 67, 2367 (1991).
- [22] H.S.J. van der Zant, F.C. Fritschy, T.P. Orlando, and J.E. Mooij, Physica (Amsterdam) 165& 166B, 969 (1990); and H.S.J. van der Zant, C.J. Müller, L.J. Geerligs, C.J.P.M. Harmans, and J.E. Mooij, Phys. Rev. B. 38, 5154 (1988).
- [23] W. Yu, and D. Stroud, Phys. Rev. B 46, 14005 (1992).
- [24] T. Baumberger, F. Heslot, and B. Perrin, Nature 367, 544 (1994).

## FIGURES

FIG .1. Array geometry used in the simulations, illustrated with an  $8 \times 8$  array. Junctions are denoted as crossed bonds. In the y-direction periodic boundaries are imposed, while the current bias is applied along the x-direction.

FIG .2.  $\eta_c = 0$  I-V characteristics, plotted as average vortex velocity versus normalized bias current. The dashed line gives the results from simulations of a  $32 \times 32$  array with one vortex. The simulation shows a vortex viscosity that decreases with increasing vortex velocity. The full line was obtained from the model vortex equation of motion (3).

FIG .3. Simulation results for the I-V characteristics as in Fig. 2 for different values of  $\eta_c$  (circles). The full lines are the fits to the I-V characteristics using Eq. (15) for a  $32 \times 32$  lattice. For clarity of presentation the origin of successive  $\eta_c$  values is offset to the right by 0.1 unit. The inset shows the values of the fitted parameters A and B as a function of  $\eta_c$  and array size. Diamonds (A) and triangles (B) correspond to  $32 \times 32$  array whereas circles (A) and squares (B) to  $16 \times 16$ .

FIG .4. Hysteresis loops in the simulated I-V characteristics for a  $4 \times 4$  array with one vortex, for different  $\eta_c$  values. Note the smallness of the current scale. First the current is swept up to  $i_b = 0.1265$ , slightly above the depinning current, and subsequently it is swept down until the vortex is retrapped by the lattice. The depinning current is  $i_b = 0.126$  for all  $\eta_c$  values shown. For  $\eta_c = 7$  the current at which the vortex is retrapped is (on this scale) equal to the depinning current. For higher values of  $\eta_c$  this current is increasingly lower. For  $8 \times 8$  and larger lattices the hysteresis for these  $\eta_c$  values disappears.

FIG .5. I-V characteristics (vortex velocity versus bias current) from simulations of a  $32 \times 32$  array with one vortex, for different values of  $\eta_c$ . From top (marked with 1') to bottom (2'),  $\eta_c = 0; 1.2; 3; 7; 15; 50; 100$ , respectively. Note that the higher  $\eta_c$ , the smaller the vortex regime. In the inset the nonlinear friction force  $F_D(\underline{y}) = A\underline{y}(1 + B\underline{y})$  (full line) is shown as a function of the vortex velocity  $\underline{y}$ , for the  $\eta_c = 0$  parameter values  $A = 2.67$  and  $B = 1.80$ . The dashed line is the friction force  $F_D(\underline{y}) = \underline{y}$  in the constant-viscosity model (3).

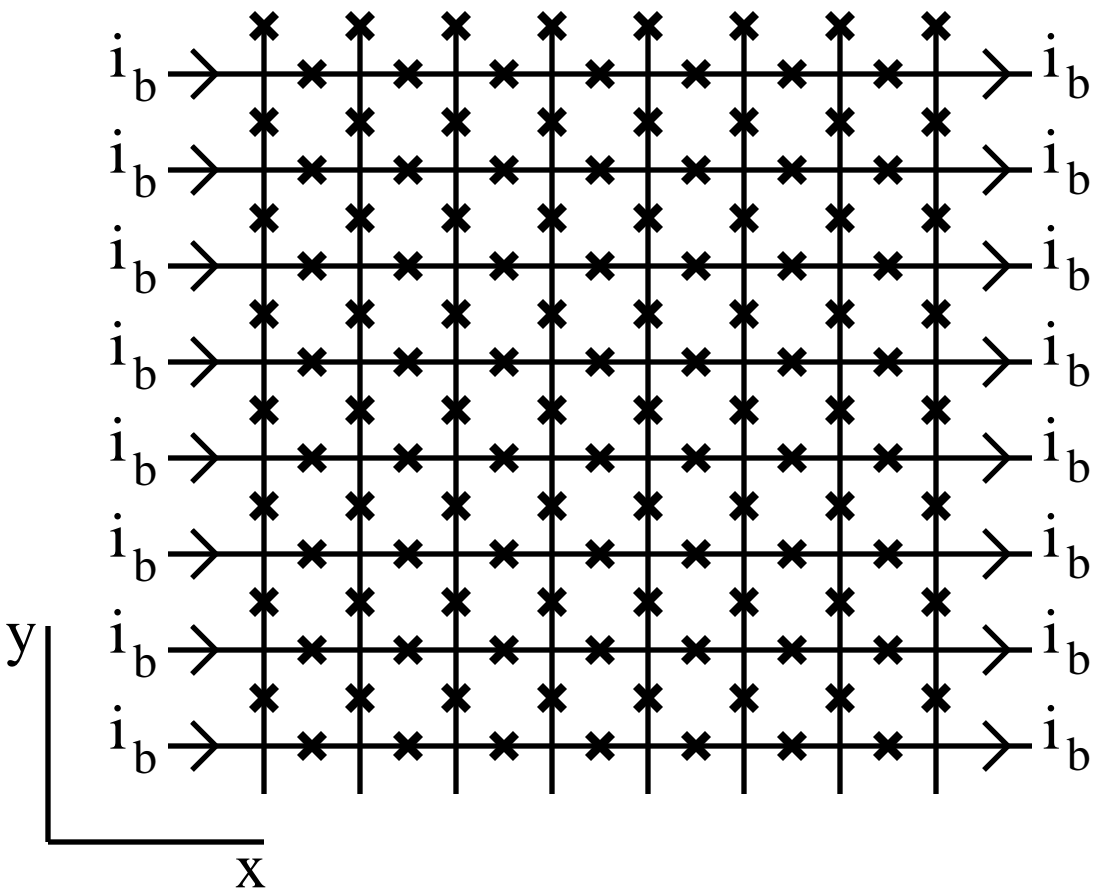
FIG .6. Simulation results from Ref. [17] for an  $8 \times 8$  triangular array with current along the [101] direction,  $\eta_c = 0$  (circles). The continuous line is the fit using Eq. (15). The fit parameters obtained are  $A = 7.67$  and  $B = 2.47$ .

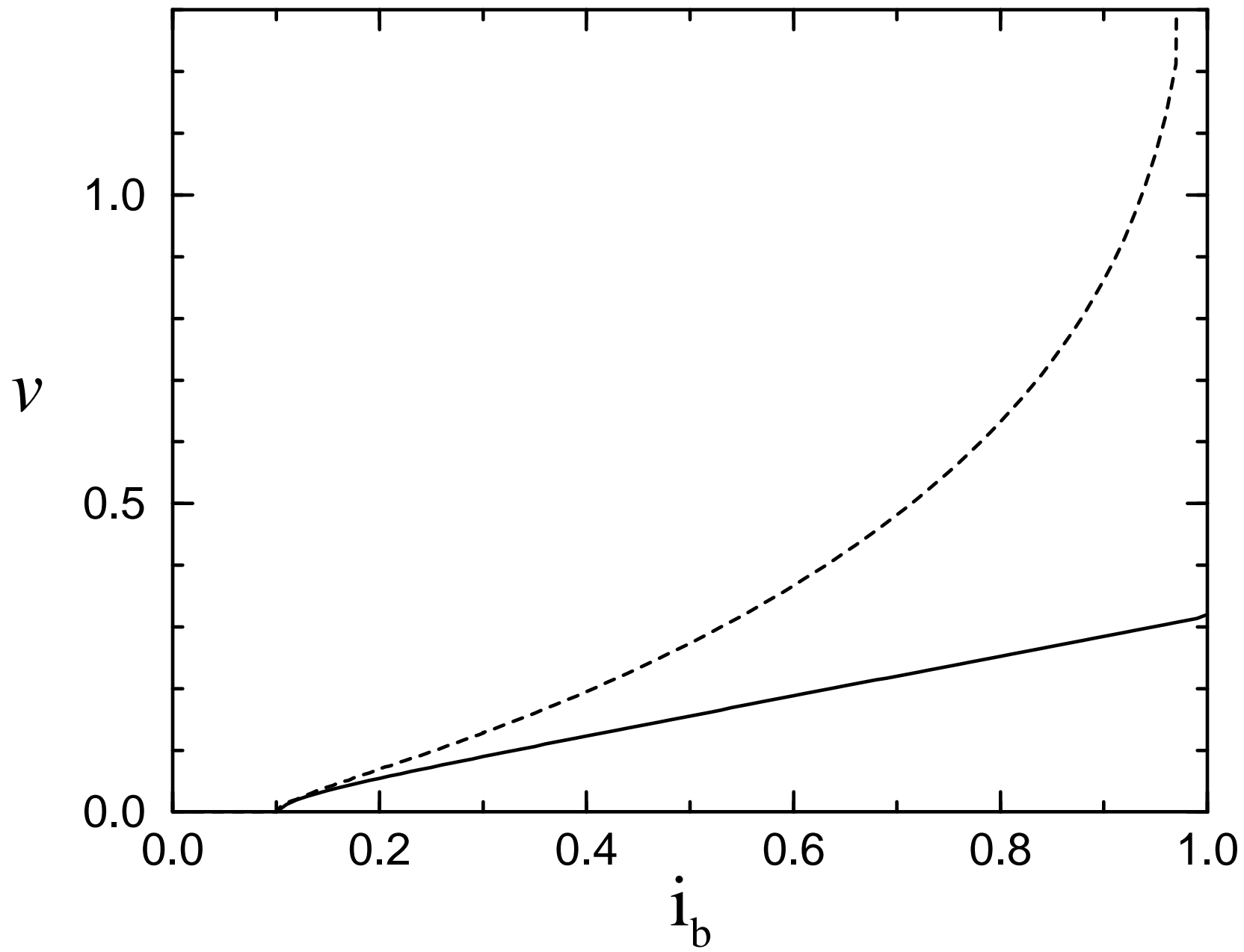
FIG. 7. Snapshots of a smooth interpolation of one vortex current vorticity distribution in an  $8 \times 8$  sublattice of a  $16 \times 16$  array, for two different current values: (a)  $i_b = 0.11$ , (b)  $i_b = 0.60$ . Different gray scales represent different levels of current vorticity. In the first snapshots (labelled as 0'), the black dot is the middle point of the vortex. The dashed line (x'ed in time) is a guide to the eye. In (a) the time interval between two snapshots is  $\Delta t = 10$  (in units of  $1/\omega_c$ ). The vortex moves over one plaquette in approximately  $t = 7 \Delta t$ . In (b) the time interval between successive snapshots is  $\Delta t = 0.625$  in units of  $1/\omega_c$ , and here the period of the motion is approximately  $t = 4.5 \Delta t$ .

FIG. 8. Rescaled voltage (full lines) and vortex center of mass velocity (dashed lines) versus time, in an  $8 \times 64$  array, for three different bias currents. The amplitude of the oscillatory component in both quantities decreases with increasing  $i_b$ .

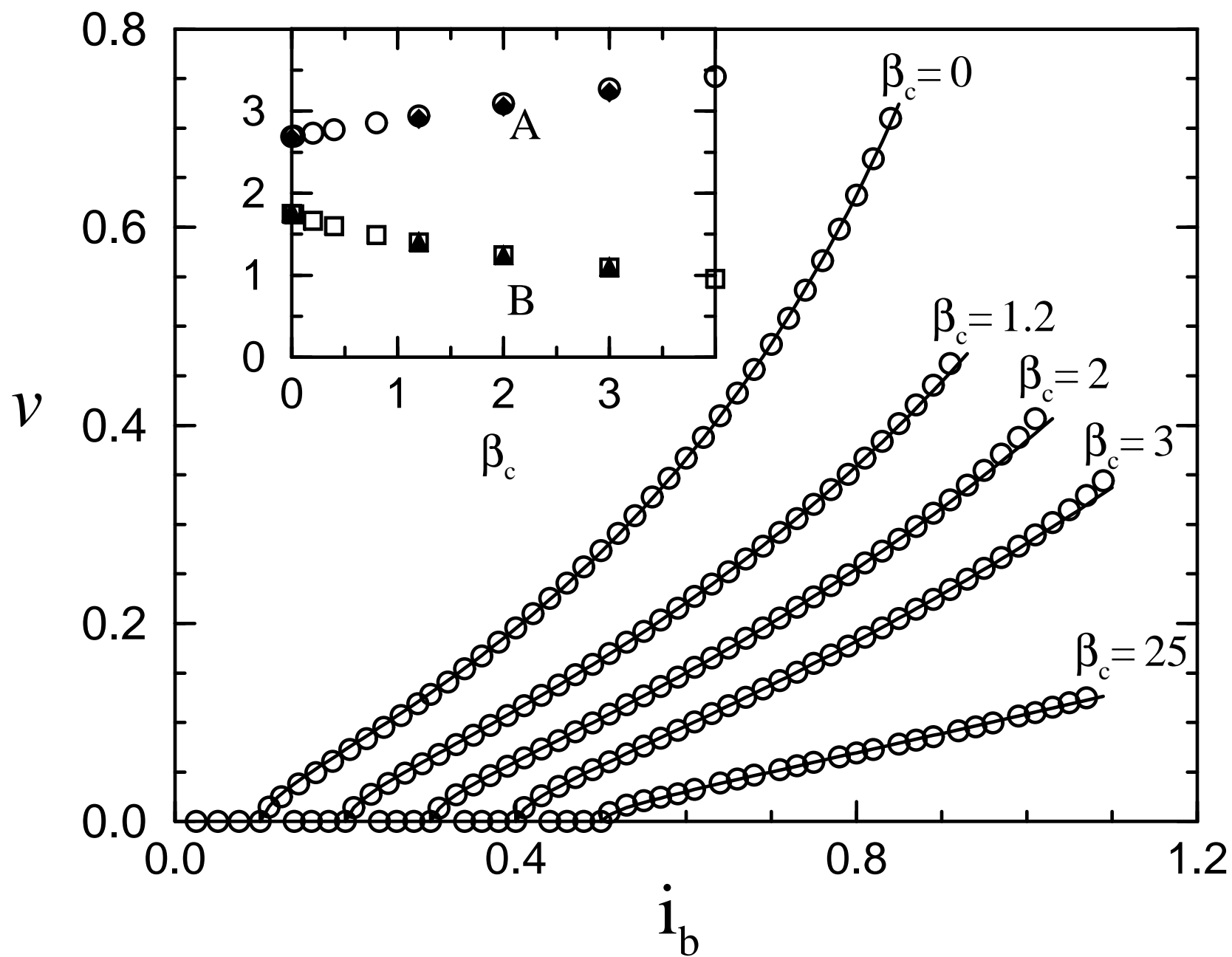
FIG. 9. Comparison of the  $\omega_c = 0$  average vortex velocity versus normalized bias current obtained from a simulation of a  $32 \times 32$  array with one vortex (dashed line) with the one from Eq. (18) (curve (a)). Curve (b) is obtained from Eq. (18) by replacing the smooth high-momentum cutoff in (18) by the sharp cutoff (19). Curve (c) is obtained from the model vortex equation of motion (3).

Hagenaars et al., Fig. 1

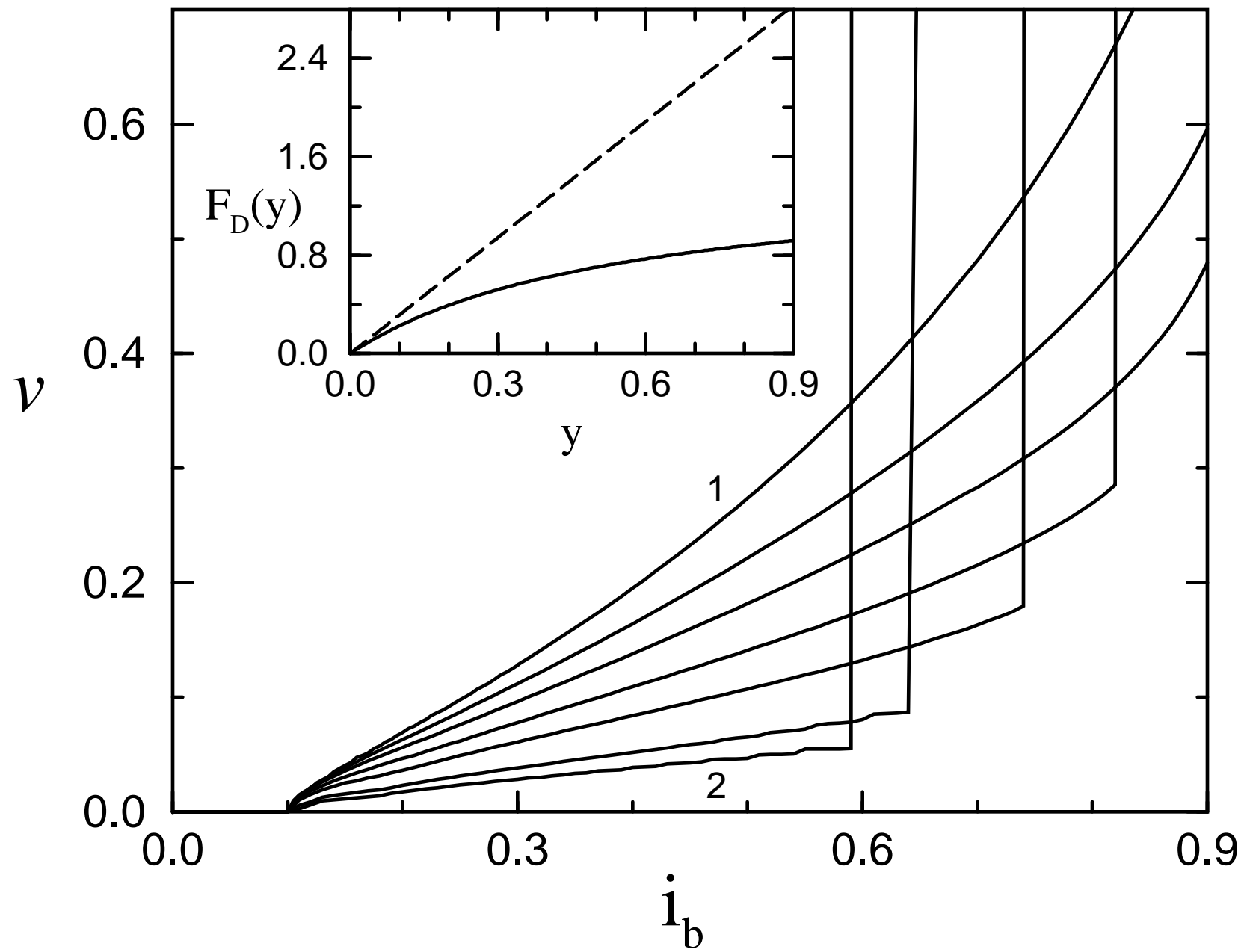


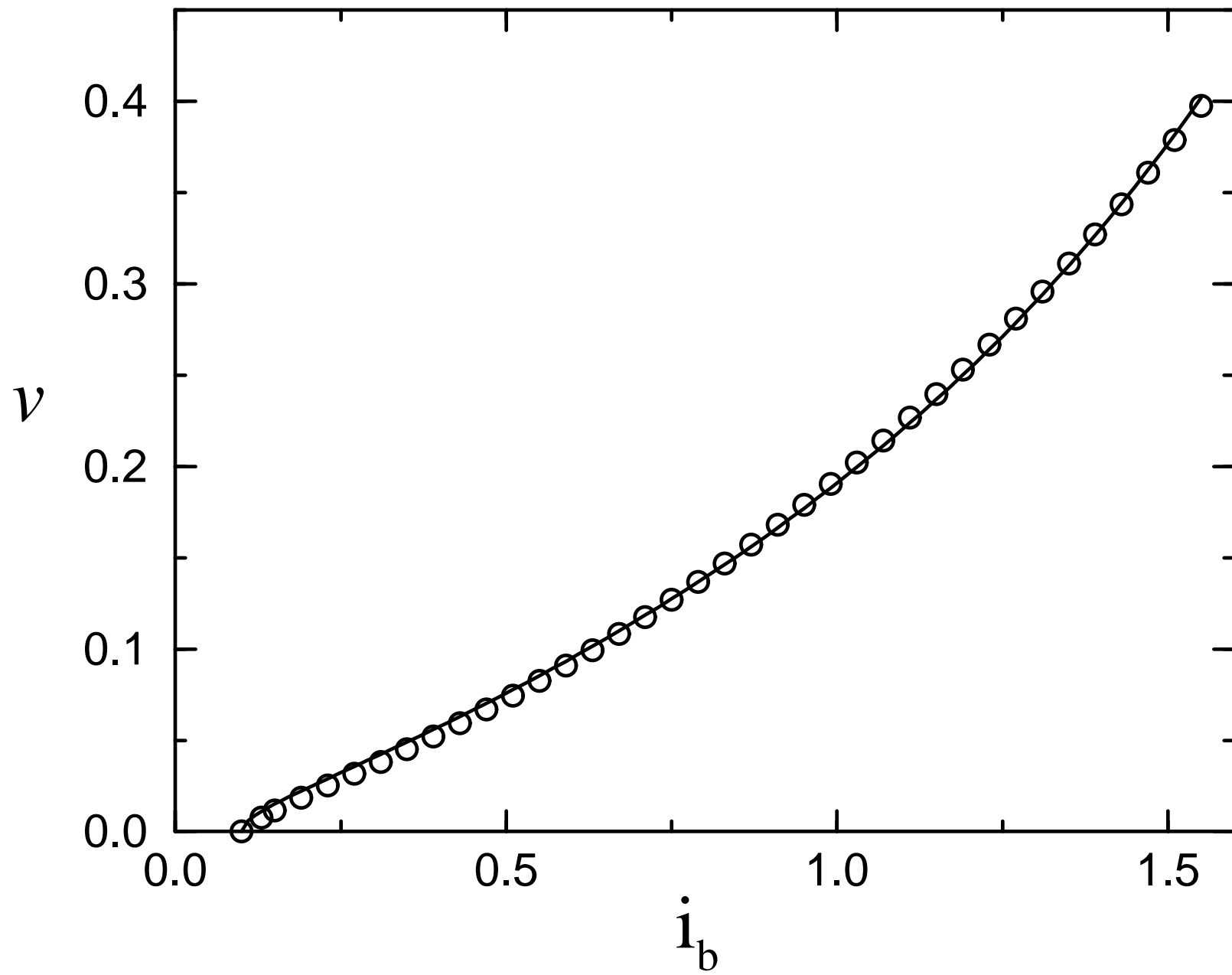




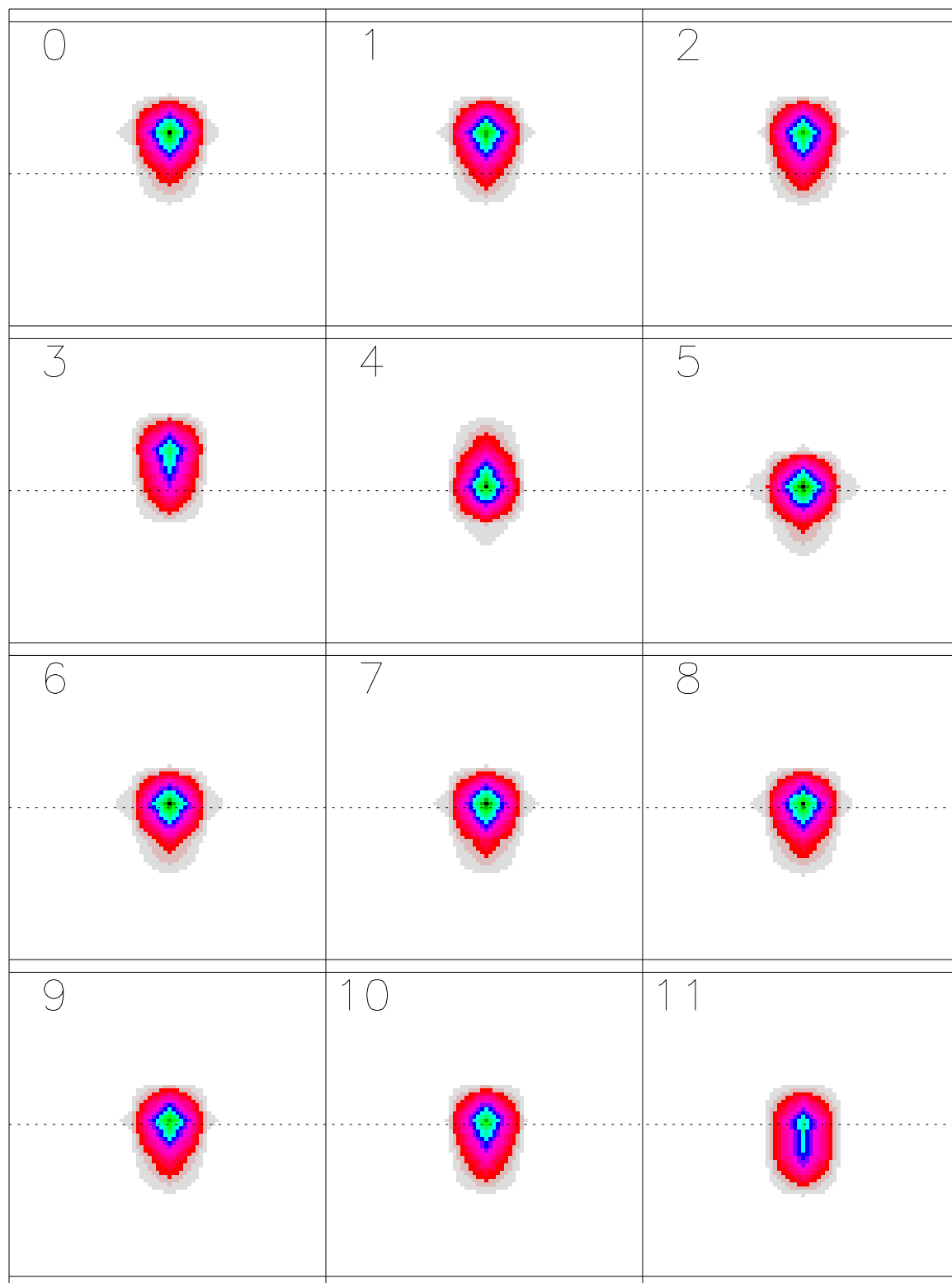








(a)



(b)

